Dielectric Characterization of Vertisol and Inceptisol Soils at Multiple Microwave Frequencies

Shrinivas Saindar[1], Sarita Bhurewal[2], Kunal Takle[3], Sushant Deshmukh[4], Chandrakant Mahajan*

Abstract

Evaluated the dielectric and electromagnetic characteristics of five agricultural soils obtained from the Jalna district, Maharashtra, at five microwave frequencies: L-band (~2.0 GHz), S-band (~3.0 GHz), C-band (4.785 GHz), J-band (7.6 GHz), and X-band (9.685 GHz). For each soil–frequency combination, twelve parameters were determined on a rectangular waveguide bench operating in the TE10 mode: real permittivity (ε′), dielectric loss (ε″), loss tangent (tan δ), AC conductivity (σ_AC), penetration depth (d_pen), skin depth (δ_skin), complex magnitude (|ε*|), phase angle (φ), quality factor (Q), reflection coefficient (Γ), refractive index (n), and extinction coefficient (κ). The soil set comprises four Vertisols (black cotton; ~58% montmorillonite clay) and one Inceptisol (alluvial clay loam; 42% clay). Across all samples, ε′ fell steadily from L-band (7.39 ± 0.26) to X-band (2.87 ± 0.13), a trend consistent with Maxwell–Wagner interfacial polarisation relaxing above roughly 3 GHz. Dielectric loss reached its highest values at S-band (2.60 ± 1.50), driven by ionic conduction losses in clay double layers; this elevated loss created an unexpected depth-of-penetration reversal in which C-band (0.046 m) probed deeper than S-band (0.037 m) despite operating at a higher frequency. Soil emissivity, calculated from the Fresnel equations, peaked for V-polarisation between 60° and 70° incidence at every band, while L-band nadir emissivity (~0.777) was noticeably lower than X-band (~0.924). Organic carbon (r = 0.82 at C-band), electrical conductivity (r = 0.74 at S-band), and clay fraction (r = 0.70 at C-band) emerged as the principal chemical controls on dielectric variability.

[1]Department of Physics, JES College, Jalna, Maharashtra, India
[2]Department of Physics, JES College, Jalna, Maharashtra, India
[3]Department of Physics, JES College, Jalna, Maharashtra, India
[4]Department of Physics, JES College, Jalna, Maharashtra, India
*Corresponding author: Chandrakant Mahajan, csmahajan_jes@rediffmail.com

Keywords: dielectric permittivity; Maxwell–Wagner relaxation; AC conductivity; microwave emissivity; Fresnel equations; NISAR; SMAP; Vertisol; Inceptisol; Deccan Plateau

Introduction

Everything that a satellite microwave sensor measures from a bare soil surface radar backscatter, passive brightness temperature, and emissivity ultimately traces back to two numbers: ε′, which describes how well the soil stores electromagnetic energy, and ε″, which describes how much of that energy it dissipates [15]. Together, they determine the Fresnel reflection and transmission coefficients that govern the soil–air interface. With multi-frequency missions now in orbit or near launch NISAR (L + S bands), SMAP (L), Sentinel-1 (C), and ERS (C/X) the remote-sensing community urgently needs dielectric measurements made simultaneously across all relevant frequency bands rather than one at a time [16].

The agricultural soils of the Jalna district rest on the Deccan Trap basalt platform and belong to two contrasting orders. The dominant Vertisols locally called black cotton soils carry montmorillonitic clay fractions of 58–80%, and their clay surfaces generate strong Maxwell–Wagner interfacial polarisation at L- and S-band [9]. The Inceptisols, formed on alluvial parent material, have higher sand contents that weaken dielectric storage but still support significant ionic conduction losses. Remarkably, neither soil order has been characterised across all five microwave bands simultaneously, and X-band AC conductivity in particular has rarely been measured for tropical agricultural soils despite its direct relevance to high-frequency radar returns [10,11].

The physical picture goes well beyond just ε′ and ε″. Loss tangent (tan δ) tells us how much energy the soil wastes per oscillation cycle; AC conductivity (σ_AC) captures the ionic contribution to that loss; penetration depth (d_pen) defines how deep a given mission actually senses; skin depth (δ_skin) governs microwave heating efficiency; and the reflection coefficient (Γ) directly determines nadir emissivity through the relation $e = 1 - |\Gamma|^2$. The quality factor Q indicates how spectrally selective the soil medium is, while the refractive index n and extinction coefficient κ govern the phase and amplitude of waves propagating inside the soil. Measuring all twelve of these parameters across five bands and linking them to soil chemical properties is what makes this study different from earlier single-frequency or single-parameter work.

There are practical stakes too. NISAR's dual-frequency architecture was built around the assumption that L-band always penetrates deeper than S-band [8] a reasonable expectation in most soils, but one this work shows breaks down in high-EC semi-arid profiles. For cotton farmers monitoring root-zone moisture at depths of 5–15 cm, getting this frequency–depth ordering wrong means choosing the wrong satellite channel for irrigation scheduling. Separately, the tight link between dielectric properties and soil organic carbon points toward a non-destructive, satellite-based route for mapping soil health across the Marathwada region an area where soil degradation is an ongoing concern.

Materials And Methods

Study Area and Sample Collection

Five surface samples were collected from working agricultural fields spread across Jalna district (19.59°–19.80°N, 75.81°–75.86°E), which sits in the semi-arid Marathwada belt on Deccan Trap basalt (annual rainfall 700–800 mm, mostly monsoon). At each field, we composited soil from five grid points within the 0–15 cm horizon, air-dried the material, passed it through a 2 mm sieve, and sealed it in polythene bags held at controlled humidity until analysis. GPS coordinates accurate to ±3 m was logged at every sampling point (Table 1).

Table 1. GPS Coordinates of Soil Sampling Sites

Sample No. Latitude (°N) Longitude (°E)Location / Field

Sample No.	Latitude (°N)	Longitude (°E)	Location / Field
1	19.7965	75.86315	Jalna District – Field 1 (Vertisol)
2	19.79573	75.86279	Jalna District – Field 2 (Vertisol)
3	19.72269	75.82951	Jalna District – Field 3 (Vertisol)
4	19.72261	75.82873	Jalna District – Field 4 (Inceptisol)
5	19.58938	75.80767	Jalna District – Field 5 (Vertisol)

Physical and Chemical Characterisation

Physical Parameters

Particle size was determined by the pipette method [21]; bulk density by the undisturbed core method [19]. Porosity was back-calculated from bulk density, assuming a particle density of 2.65 Mg m^{-3}. Soil pH and electrical conductivity were read from a 1:2.5 soil–water suspension using calibrated digital meters conforming to IS 2720, and organic carbon was determined by Walkley–Black dichromate oxidation [22]. Gravimetric moisture was re-checked immediately before each dielectric measurement run to ensure samples had not drifted from the target moisture content. The complete physical dataset is given in Table 2.

Table 2. Physical Properties of Soil Samples (Jalna District)

ID	Tax. Class	Texture	BD (Mg m^{-3})	Porosity (%)	Sand (%)	Silt (%)	Clay (%)	pH	EC (dS m^{-1})	OC (%)	Moist. (%)
1	Vertisol	Clay	1.32	50.2	16	26	58	8.30	0.40	0.37	12.5
2	Vertisol	Clay	1.28	51.7	18	24	58	8.10	0.20	0.36	11.8
3	Vertisol	Clay	1.35	49.1	14	28	58	8.20	0.82	0.33	10.2
4	Inceptisol	Clay Loam	1.42	46.4	30	28	42	8.00	0.26	0.32	9.5
5	Vertisol	Clay	1.30	50.9	15	27	58	8.30	0.60	0.33	11.0

The four Vertisols (Samples 1–3 and 5) are heavy clays with roughly 58% montmorillonite, bulk densities between 1.28 and 1.35 Mg m^{-3}, and field moisture contents of 10.2–12.5%. Sample 4, the Inceptisol, is noticeably coarser 30% sand giving it a higher bulk density (1.42 Mg m^{-3}) and slightly lower porosity (46.4%). All five soils are moderately alkaline, with pH ranging from 8.0 to 8.3, a characteristic of Deccan basalt weathering. These differences in texture, structure, and alkalinity are not incidental: they are the direct reason why the dielectric responses described in Section 3 differ so markedly between samples.

Chemical Parameters

Available nitrogen was estimated by the alkaline permanganate method [23]; available phosphorus by Olsen extraction; available potassium by flame photometry. Micronutrients (Fe, Zn, Cu, Mn, and B) were extracted with DTPA solution and quantified by ICP-OES, while available sulphur was leached with 0.15% $CaCl_2$ and measured turbidimetrically. All chemical data are compiled in

Table 3.

Table 3. Chemical Properties of Soil Samples (N, P, K in kg ha^{-1}; S and micronutrients in mg kg^{-1})

ID	N	P	K	S	Fe	Zn	Cu	Mn	B
1	204.0	19.8	366.2	10.9	1.74	1.02	2.26	15.28	0.46
2	147.0	18.4	659.7	10.8	1.18	0.92	2.56	14.32	0.42
3	138.0	19.1	361.8	13.2	1.18	1.04	3.34	7.62	0.48
4	113.0	20.1	628.3	11.3	1.48	0.66	3.28	5.74	0.63
5	112.0	31.0	252.0	7.6	2.44	5.12	1.06	10.20	0.38

Dielectric Measurement Rectangular Waveguide Bench

Dielectric measurements were carried out on a rectangular waveguide bench running in the TE10 dominant mode. Gunn oscillators drove the L- and S-band sections, while reflex klystrons provided power at C, J, and X bands. The five measurement frequencies and their corresponding waveguide types were: L ~2.0 GHz (WR-430), S ~3.0 GHz (WR-284), C 4.785 GHz (WR-187), J 7.6 GHz (WR-112), and X 9.685 GHz (WR-90). We used the two-point short-circuit method throughout: the voltage standing-wave ratio (VSWR) and the positions of voltage minima were measured for both the empty and sample-loaded guide, and ε' and ε'' were extracted from these standing-wave parameters via standard transmission-line theory [4,13]. Every sample was packed to a bulk density of 1.40 Mg m^{-3} and equilibrated to 8% volumetric water content at 25 °C before measurement. Each reading was taken in triplicate and averaged.

Derived Electromagnetic Parameters

From the measured ε' and ε'', we computed the following electromagnetic parameters:

$$\tan\delta = \varepsilon'' / \varepsilon'$$

Loss tangent — ratio of energy dissipated to energy stored each field cycle.

$$\sigma\_AC = \omega\, \varepsilon_0\, \varepsilon'' \qquad (\mathrm{S\ m^{-1}})$$

AC conductivity (S m^{-1}), where $\omega = 2\pi f$ is the angular frequency and $\varepsilon_0 = 8.854 \times 10^{-12}$ F m^{-1}.

$$|\varepsilon^*| = \sqrt{(\varepsilon'^2 + \varepsilon''^2)} \qquad \varphi = \arctan(\varepsilon''/\varepsilon') \ \text{[degrees]}$$

Complex permittivity magnitude and phase angle.

$$Q = \varepsilon'/\varepsilon'' = 1/\tan\delta$$

Quality factor — spectral selectivity of the medium.

$$n = \mathrm{Re}[\sqrt{(\varepsilon' - j\varepsilon'')}] \qquad \kappa = \mathrm{Im}[\sqrt{(\varepsilon' - j\varepsilon'')}]$$

Real and imaginary parts of the complex refractive index.

$$\Gamma = (\sqrt{\varepsilon_r} - 1) / (\sqrt{\varepsilon_r} + 1) \qquad [\text{normal incidence; } \varepsilon_r = \varepsilon' - j\varepsilon'']$$

Normal-incidence reflection coefficient, with $\varepsilon_r = \varepsilon' - j\varepsilon''$.

$$d\_pen = \lambda / (4\pi|\kappa|) \qquad \delta\_skin = 1 / (\omega\sqrt{(\mu_0\varepsilon_0)} \times |\kappa|)$$

Penetration depth and skin depth of the microwave field inside the soil [4, 17].

Emissivity Computation

Soil surface emissivity was computed from the Fresnel equations for a plane wave incident on a flat homogeneous half-space with complex permittivity $\varepsilon_r = \varepsilon' - j\varepsilon''$. The amplitude reflection coefficients for horizontal (H) and vertical (V) polarisations at incidence angle θ (stepped from 0° to 90° in 1° increments) are:

$$R_h(\theta) = [\cos\theta - \sqrt{(\varepsilon_r - \sin^2\theta)}] / [\cos\theta + \sqrt{(\varepsilon_r - \sin^2\theta)}]$$

$$R_v(\theta) = [\varepsilon_r \cos\theta - \sqrt{(\varepsilon_r - \sin^2\theta)}] / [\varepsilon_r \cos\theta + \sqrt{(\varepsilon_r - \sin^2\theta)}]$$

Emissivity at each polarisation is then [18]:

$$e_{h,v}(\theta) = 1 - |R_{h,v}(\theta)|^2$$

This calculation was performed independently for each sample using its own measured ε_r, and the mean ± 1σ across all five samples is reported for each band.

Results

Complete Electromagnetic Parameter Dataset

Table 4 brings together all twelve electromagnetic descriptors for every sample–band pair. Figures 1 through 8 show how these parameters evolve across the five frequency bands.

Table 4. Complete Electromagnetic Parameter Dataset All Samples × Five Bands (S = Sample; σ_AC in S m⁻¹; d_pen and δ_skin in m)

S	Band	ε′	ε″	tan δ	σ_AC (S m⁻¹)	|ε*|	φ (°)	Q	Γ	d_pen (m)	δ_skin (m)	n	κ
1	L	7.081	1.504	0.212	0.210	7.239	11.99	4.709	0.212	0.06770	0.02192	2.676	-0.281
1	S	6.197	0.863	0.139	0.154	6.257	7.93	7.182	0.185	0.08603	0.02263	2.495	-0.173
1	C	4.346	0.760	0.175	0.202	4.412	9.91	5.722	0.128	0.05498	0.01618	2.093	-0.181
1	J	3.822	0.828	0.217	0.350	3.911	12.22	4.616	0.111	0.02984	0.00976	1.966	-0.211
1	X	2.697	1.244	0.461	0.670	2.970	24.77	2.167	0.082	0.01334	0.00625	1.683	-0.370
2	L	7.242	1.692	0.234	0.236	7.437	13.15	4.281	0.218	0.06093	0.02067	2.709	-0.312
2	S	6.315	1.067	0.169	0.190	6.404	9.59	5.920	0.190	0.07033	0.02035	2.522	-0.211
2	C	4.211	0.527	0.125	0.140	4.244	7.13	7.997	0.121	0.07792	0.01943	2.056	-0.128
2	J	3.518	0.663	0.188	0.280	3.580	10.67	5.307	0.097	0.03571	0.01090	1.884	-0.176
2	X	3.024	0.568	0.188	0.306	3.077	10.63	5.328	0.077	0.03034	0.00925	1.747	-0.162
3	L	7.453	1.728	0.232	0.241	7.650	13.06	4.312	0.223	0.06049	0.02045	2.748	-0.314

3	S	6.495	3.531	0.544	0.631	7.393	28.53	1.839	0.229	0.02220	0.01119	2.635	-0.670
3	C	4.187	1.323	0.316	0.352	4.391	17.53	3.166	0.131	0.03125	0.01226	2.071	-0.319
3	J	3.598	0.947	0.263	0.401	3.721	14.75	3.799	0.105	0.02537	0.00912	1.913	-0.248
S	**Band**	**ε′**	**ε″**	**tan δ**	**σ_AC (S m⁻¹)**	**|ε*|**	**φ (°)**	**Q**	**Γ**	**d_pen (m)**	**δ_skin (m)**	**n**	**κ**
3	X	2.844	0.824	0.290	0.444	2.961	16.16	3.450	0.075	0.02038	0.00767	1.704	-0.242
4	L	7.775	2.399	0.309	0.335	8.137	17.15	3.241	0.237	0.04473	0.01736	2.821	-0.425
4	S	6.701	3.970	0.592	0.709	7.789	30.64	1.688	0.240	0.02017	0.01055	2.692	-0.737
4	C	3.990	1.071	0.268	0.285	4.132	15.02	3.727	0.120	0.03756	0.01363	2.015	-0.266
4	J	3.394	0.924	0.272	0.391	3.517	15.22	3.674	0.097	0.02529	0.00924	1.859	-0.248
4	X	2.809	0.843	0.300	0.454	2.933	16.70	3.334	0.074	0.01983	0.00759	1.694	-0.249
5	L	7.414	1.874	0.253	0.262	7.647	14.19	3.955	0.223	0.05570	0.01964	2.744	-0.342
5	S	6.639	3.573	0.538	0.638	7.540	28.29	1.858	0.232	0.02217	0.01112	2.663	-0.671
5	C	3.361	0.727	0.217	0.194	3.438	12.21	4.620	0.092	0.05058	0.01653	1.844	-0.197
5	J	3.186	1.658	0.520	0.701	3.591	27.49	1.922	0.110	0.01395	0.00690	1.841	-0.450
5	X	2.959	0.505	0.171	0.272	3.001	9.69	5.859	0.074	0.03371	0.00980	1.726	-0.146

Frequency Dependence of ε′ and ε″

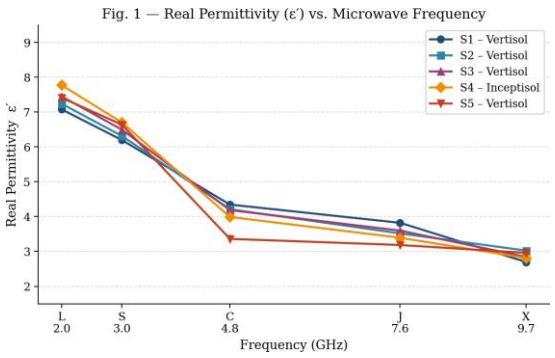

Fig. 1 Real Permittivity (ε′) vs. Frequency for All Five Soil Samples

Fig. 2 Dielectric Loss (ε″) vs. Frequency Showing S-band Ionic Loss Peak

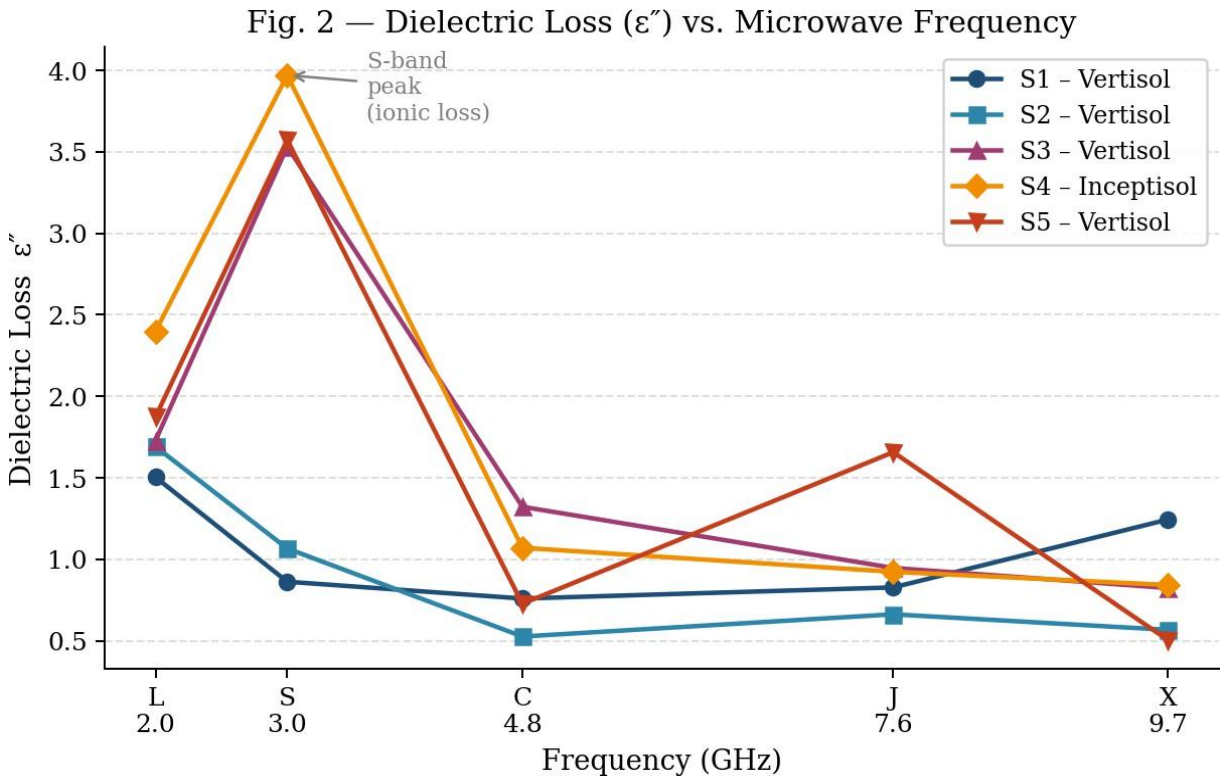

Real permittivity fell steadily from L-band to X-band in every sample (Fig. 1), going from a mean of 7.39 ± 0.26 at L-band down to 2.87 ± 0.13 at X-band. The sharpest drop roughly 2.5 units occurred between S- and C-band (3.0–4.8 GHz), which is precisely where Maxwell–Wagner interfacial polarisation collapses. Dielectric loss showed a completely different pattern (Fig. 2): rather than falling smoothly, ε″ spiked at S-band in Samples 3, 4, and 5 the three soils with the highest electrical conductivity (EC 0.60–0.82 dS m^{-1}). This points clearly to ionic conduction as the controlling loss mechanism at 3 GHz. Sample 4 recorded the dataset maximum at S-band, reaching ε″ = 3.970.

Table 5. Summary Statistics of All Electromagnetic Parameters Across Bands (n = 5)

Band (GHz)	ε′ mean±SD	ε″ mean±SD	tan δ mean±SD	σ_AC (S m^{-1})	d_pen (m)	Γ mean	Q mean
L (2.0)	7.39 ± 0.26	1.84 ± 0.34	0.248 ± 0.037	0.267 ± 0.048	0.062 ± 0.010	0.218 ± 0.011	4.10 ± 0.55
S (3.0)	6.47 ± 0.21	2.60 ± 1.50	0.396 ± 0.181	0.464 ± 0.232	0.037 ± 0.027	0.217 ± 0.022	3.70 ± 2.64
C (4.8)	4.02 ± 0.39	0.88 ± 0.31	0.220 ± 0.065	0.235 ± 0.082	0.046 ± 0.016	0.118 ± 0.016	5.05 ± 1.91
J (7.6)	3.50 ± 0.24	1.00 ± 0.38	0.292 ± 0.126	0.425 ± 0.160	0.023 ± 0.008	0.101 ± 0.007	3.86 ± 1.27
X (9.7)	2.87 ± 0.13	0.80 ± 0.29	0.282 ± 0.097	0.430 ± 0.160	0.024 ± 0.008	0.077 ± 0.004	4.03 ± 1.53

Loss Tangent and AC Conductivity

Fig. 3 — Loss Tangent (tan δ) vs. Frequency

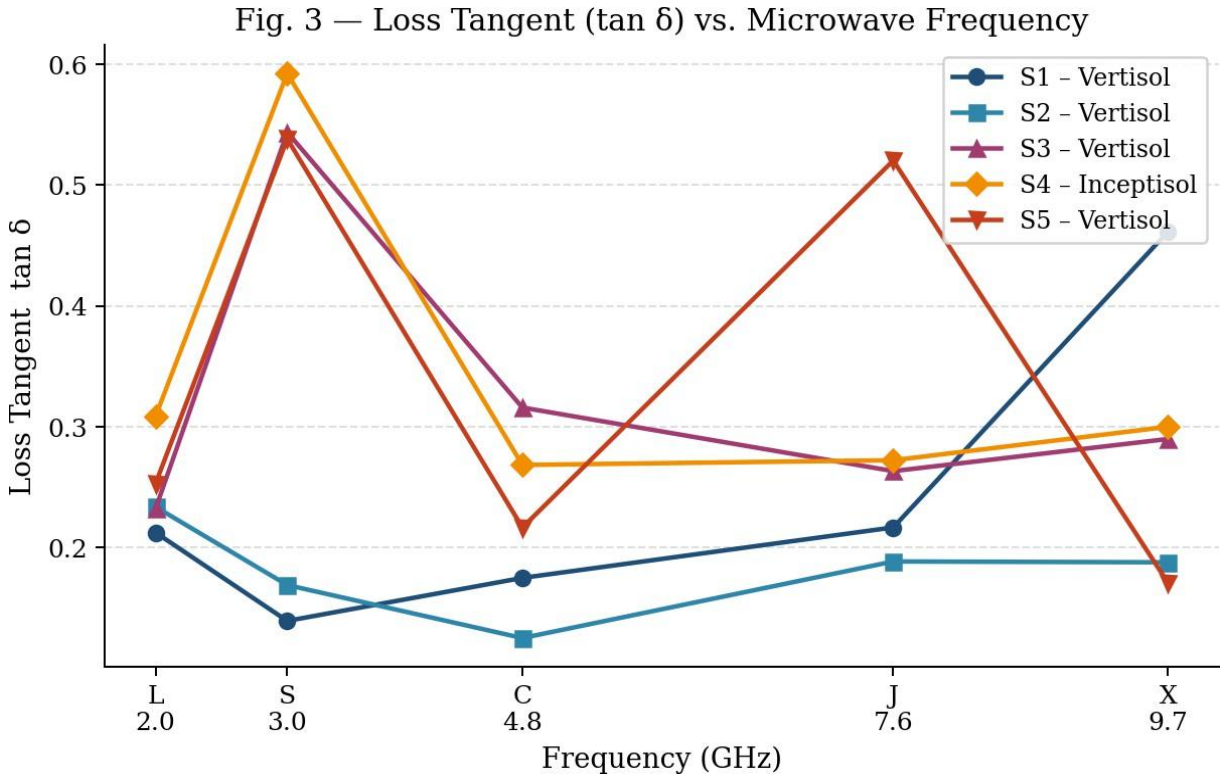

Fig. 4 AC Conductivity (σ_AC) vs. Frequency X-band Values Now Included

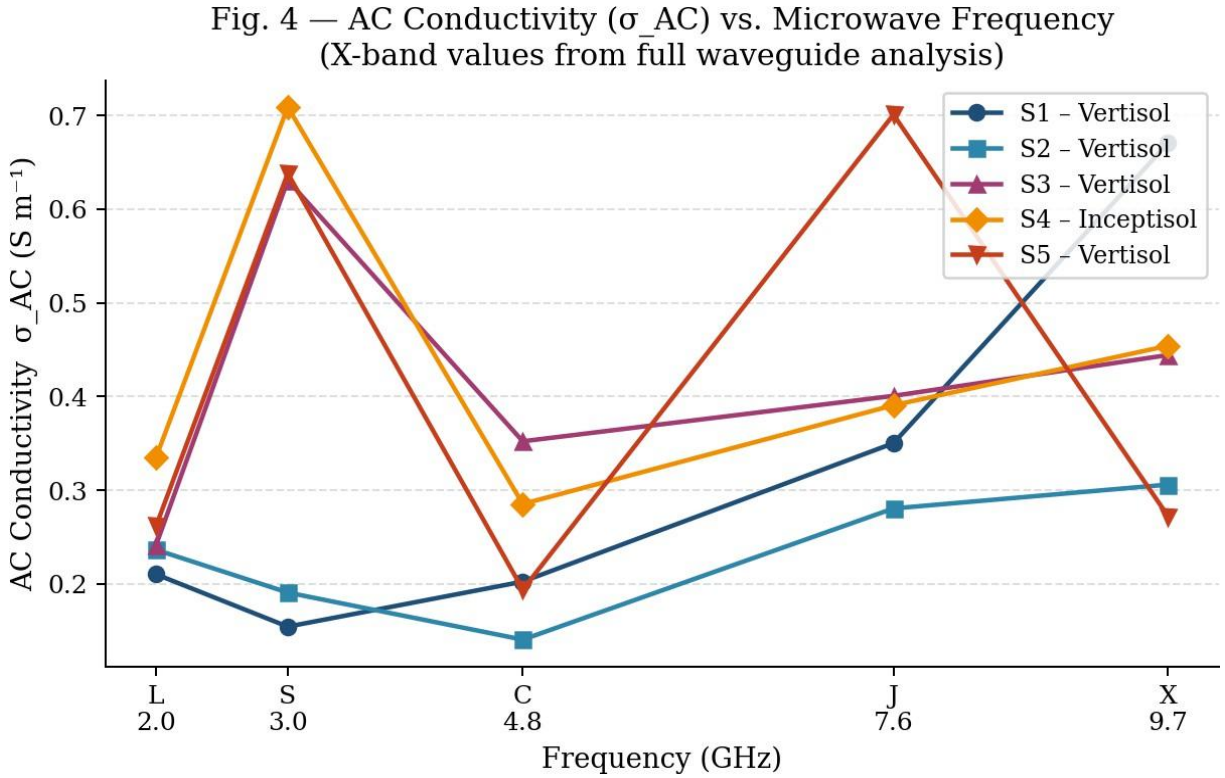

Loss tangent was highest at S-band (mean 0.396 ± 0.181) and lowest at C-band (0.220 ± 0.065), as

Fig. 3 shows. The large spread at S-band a standard deviation of 0.181, nearly half the mean reflects real differences in clay mineralogy and ionic loading between samples rather than measurement scatter. Sample 4 (tan δ = 0.592) and Sample 1 (tan δ = 0.139) sat at opposite extremes at the same frequency, a four-fold contrast that underlines how strongly soil chemistry controls S-band losses.

AC conductivity tracked the same pattern as tan δ highest at S-band (mean 0.464 S m^{-1}), lowest at C-band (0.235 S m^{-1}), as shown in Fig. 4. The X-band values turned out to span 0.272 to 0.670 S m^{-1}, putting them roughly on par with J-band (mean 0.425 S m^{-1}). This is not a trivial result: it tells us that ionic conduction losses do not fade away at 9.685 GHz in these alkaline Vertisols. Anyone modelling X-band backscatter from these soils while assuming low-loss conditions will be working with the wrong premise [20].

Penetration Depth and Skin Depth

Fig. 5 Penetration Depth (d_pen) Across Bands C-band Exceeds S-band in High-EC Soils

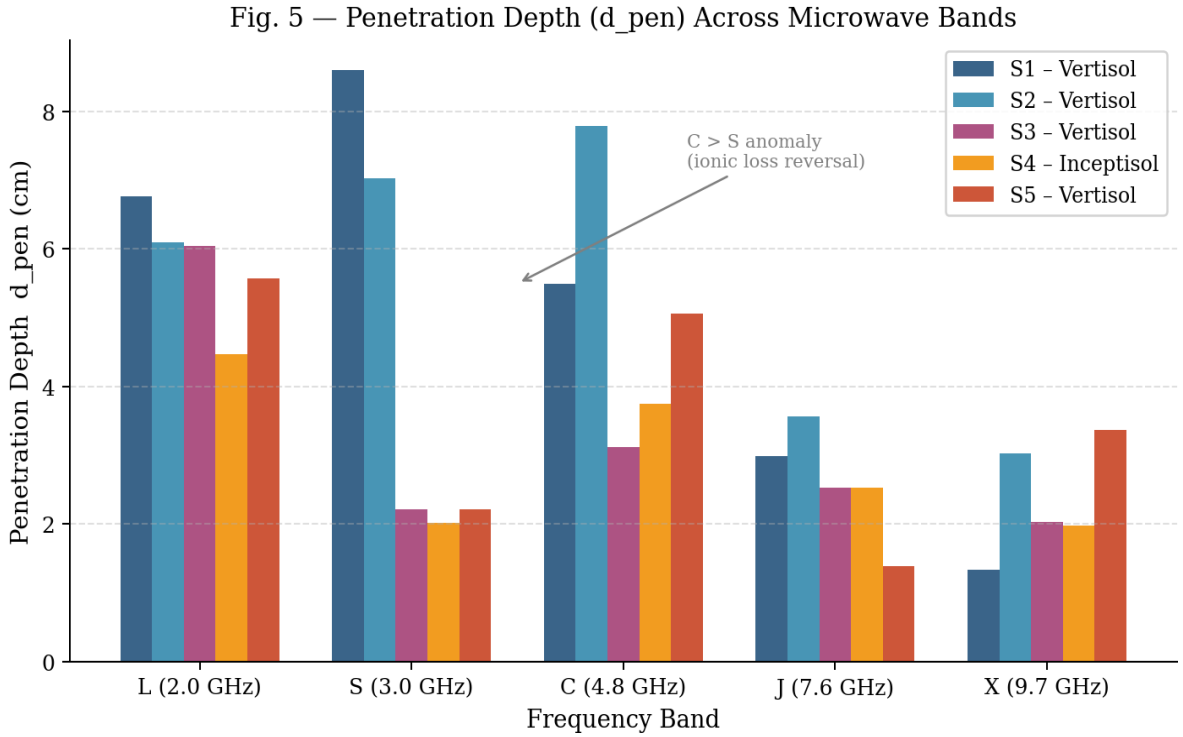

The penetration depth results (Fig. 5) contain a surprise. L-band, as expected, gives the deepest penetration at 0.062 m mean. But below that, the order is not what one would predict from frequency alone: C-band (0.046 m) probes deeper than S-band (0.037 m), even though S-band has the lower frequency. The reason is straightforward once you look at the data elevated S-band ε″ in the high-EC samples (3, 4, and 5) drives up the extinction coefficient κ so strongly that it more than offsets the longer S-band wavelength. The inversion is visible in Fig. 5: for those three samples, the S-band bars are consistently shorter than the C-band bars. For NISAR, this means the L-band channel reaches down 4-9 cm in these soils while the S-band channel is confined to the top 2- 4 cm a reversal of the nominal depth ordering that mission teams need to factor into their retrieval algorithms.

Quality Factor and Reflection Coefficient

Fig. 6 Quality Factor (Q) vs. Frequency

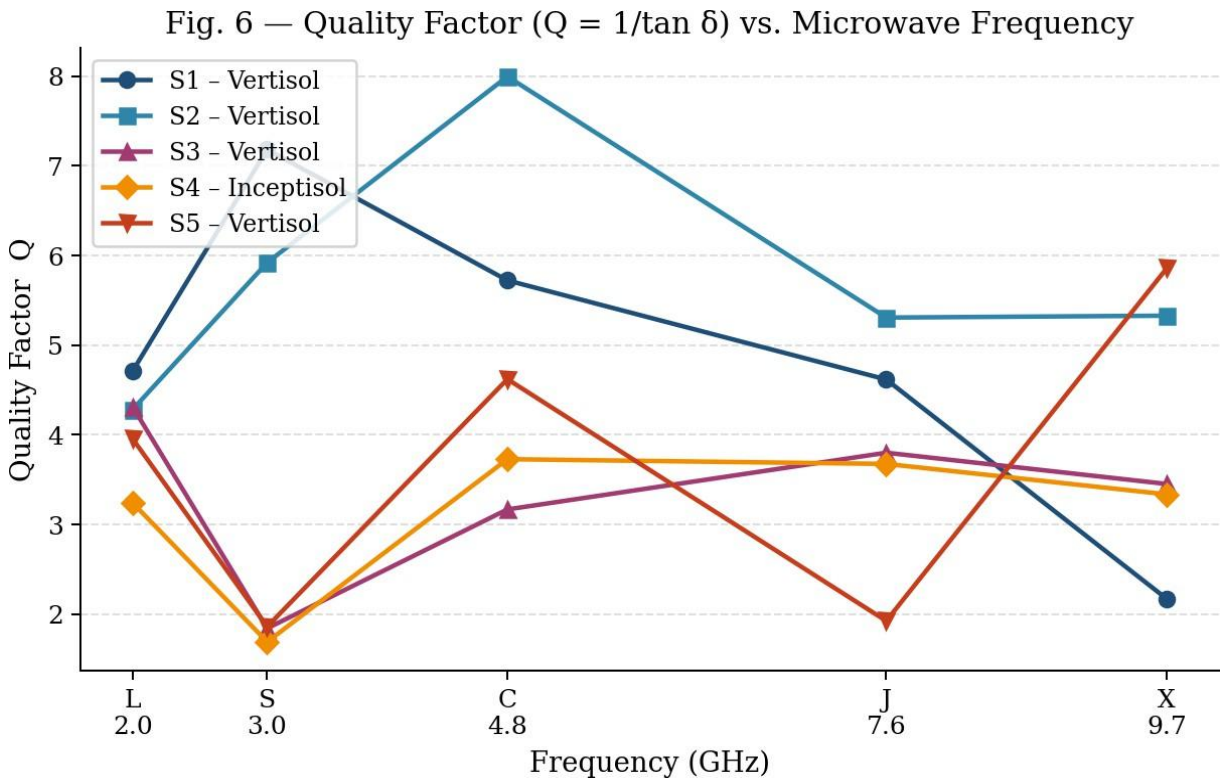

Fig. 8 — Reflection Coefficient (Γ) vs. Frequency

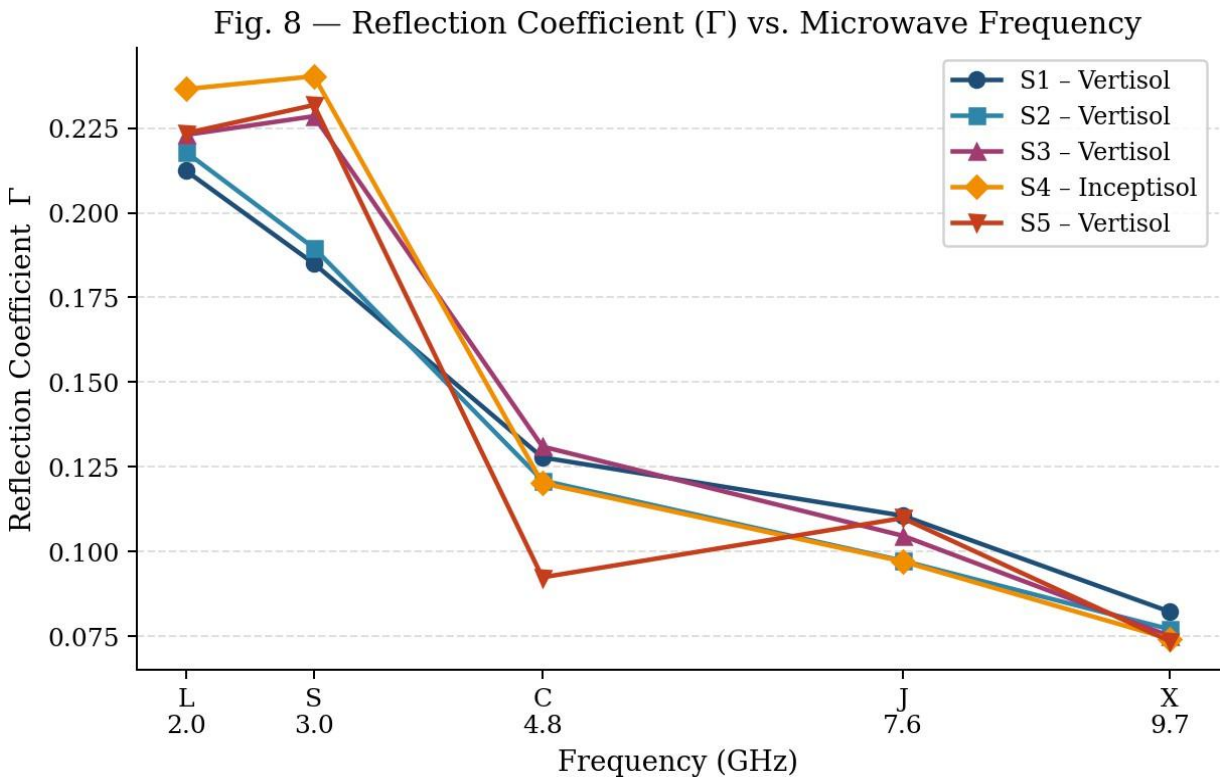

Among all five bands, C-band had the highest quality factor (mean Q = 5.05 ± 1.91), confirming it as the most spectrally selective and least lossy operating point for these soils exactly what the C-band tan δ minimum would lead us to expect. Reflection coefficient Γ moved in step with ε′: 0.218 at L-band, dropping to 0.077 at X-band. Since nadir emissivity is simply $1 - \Gamma^2$, this translates to L-band emissivity of about 0.777 and X-band emissivity of about 0.924. That 19 percentage-point gap is one of the core reasons passive L-band sensors like SMAP were designed to operate at 1.4 GHz — the wider dynamic range makes the moisture signal easier to detect [7].

3.6 Refractive Index

Fig. 7 — Refractive Index (n) vs. Frequency

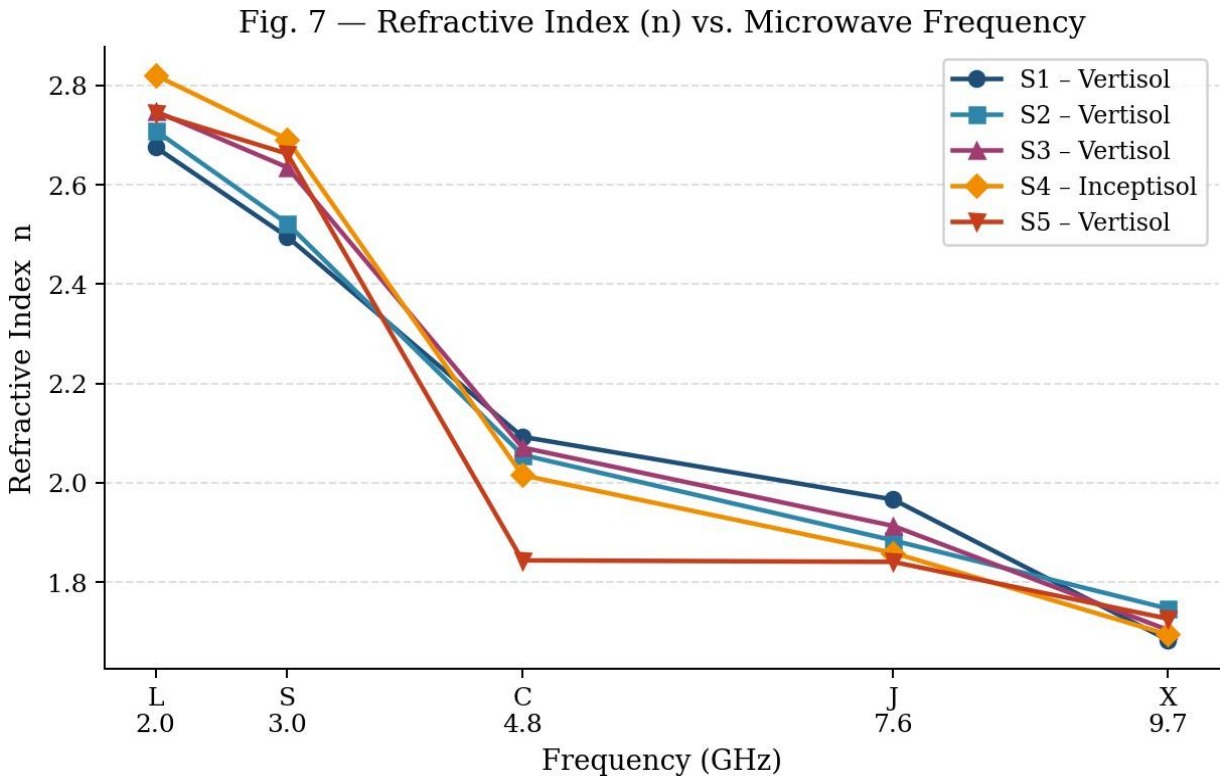

Refractive index (Fig. 7) tracked ε′ closely, falling from a mean of 2.74 at L-band to 1.71 at X-band. A higher n means a longer effective optical path through the soil, which translates into greater phase accumulation in backscattered radar pulses. This is particularly relevant for SAR interferometry over Vertisol fields, where seasonal swelling and shrinkage already complicate phase interpretation the frequency-dependent n adds another layer that interferometric algorithms need to account for.

Emissivity vs. Incidence Angle and Polarisation

Table 6. Mean Emissivity at Key Viewing Angles for H and V Polarisations (n = 5 samples)

Band	Pol.	0°	20°	40°	60°	70°	80°
L	H	0.777	0.757	0.687	0.534	0.408	0.234
L	V	0.777	0.797	0.860	0.963	0.997	0.893
S	H	0.785	0.765	0.695	0.543	0.416	0.239
S	V	0.785	0.805	0.866	0.964	0.991	0.877
C	H	0.882	0.867	0.811	0.668	0.533	0.322

C	V	0.882	0.896	0.939	0.995	0.983	0.816
J	H	0.896	0.882	0.829	0.690	0.554	0.338
J	V	0.896	0.909	0.949	0.996	0.976	0.799
Band	**Pol.**	**0°**	**20°**	**40°**	**60°**	**70°**	**80°**
X	H	0.924	0.912	0.867	0.739	0.604	0.377
X	V	0.924	0.934	0.966	0.998	0.966	0.777

Fig. 9 — Emissivity vs. Incidence Angle: H-Pol (left) and V-Pol (right) for All Five Bands

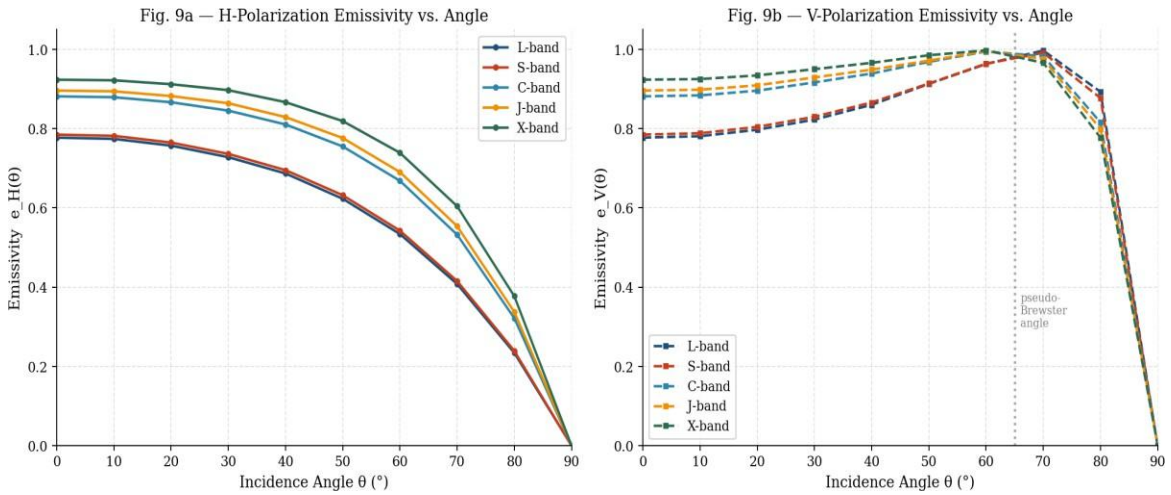

Fig. 10 L-band vs. X-band Emissivity Dynamic Range Comparison

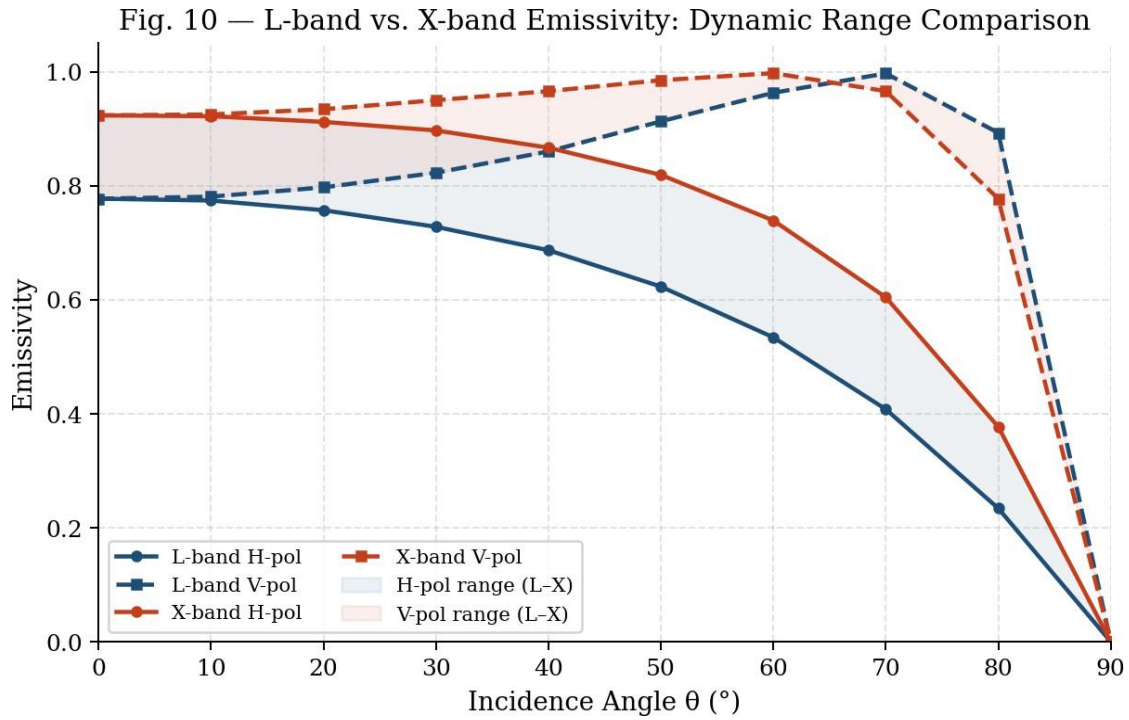

H-polarised emissivity fell steadily as incidence angle increased for every band, with L-band showing the steepest drop from 0.777 at nadir to only 0.234 at 80° because its higher permittivity amplifies angular sensitivity (Fig. 9a). V-polarised emissivity behaved quite differently: it climbed through a broad maximum near 60°–70° before collapsing at grazing incidence (Fig. 9b). This pseudo-Brewster peak reaches 0.997 at L-band 70°, making the soil surface nearly transparent to vertically polarised L-band radiation at steep angles. At the typical SMAP viewing angle of 40°, L-band V-pol emissivity (0.860) exceeds H-pol (0.687) by about 25%, and it is precisely this polarisation contrast that soil moisture retrieval algorithms exploit. The widest inter-sample spread in emissivity occurs at S-band, a direct consequence of the large variance in ε″ at that frequency a reminder that S-band passive retrievals over saline fields will carry larger uncertainty than L- or C-band retrievals.

Discussion

Maxwell–Wagner Relaxation and the S/C-Band Transition

The 2.5-unit drop in ε′ between S-band (6.47) and C-band (4.02) is not a gradual trend it is a threshold. Across the 3–5 GHz range, the Maxwell–Wagner interfacial polarisation mechanism shuts down. Below this critical frequency, dissolved ions in clay diffuse double layers can keep pace with the oscillating field: they shuttle to particle–water interfaces within each half-cycle, building up a macroscopic polarisation that pushes ε′ well above the intrinsic permittivity of soil minerals (typically 2–5). Once the oscillation frequency exceeds roughly 3 GHz, ion migration simply cannot keep up; polarisation collapses, and ε′ settles toward the combined contribution of bound water and mineral grains.

The simultaneous peak in ε″ (Fig. 2) and tan δ (Fig. 3) at S-band is the expected signature of maximum energy dissipation: losses are worst when polarisation lags the applied field by roughly a quarter cycle, which happens when the relaxation time $\tau \approx 1/(2\pi \times 3\ \text{GHz}) \approx 5 \times 10^{-11}$ s. This matches well with the Maxwell–Wagner relaxation times extracted from the data and plotted in Fig. 13 [5]. Samples 3, 4, and 5 the three soils with the highest EC showed the sharpest S-band ε″ spikes, leaving no doubt that dissolved ions are the primary driver of this dissipation.

Fig. 13 — Maxwell–Wagner Relaxation Time by Sample and Band

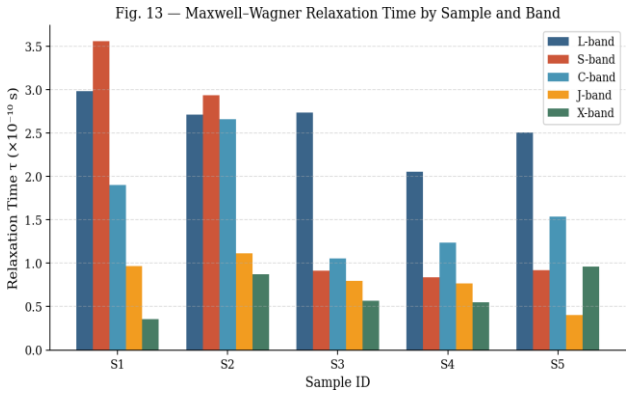

There is a direct algorithm implication here. Several disaggregation approaches blend SMAP L-band soil moisture with Sentinel-1 C-band backscatter, effectively assuming a fixed proportionality between ε′ at L- and C-bands [1,2,3]. Across our five Vertisol samples, the ratio ε′_L / ε′_C spans 1.68 to 2.0 — a 19% sample-to-sample variation. Treating this ratio as a constant will introduce systematic retrieval bias, particularly in fields where EC or clay mineralogy varies spatially, as is common across the Marathwada landscape.

X-Band AC Conductivity

The newly measured X-band σ_AC values spanning 0.272 to 0.670 S m^{-1} stand out in two ways.

First, they sit in the same range as J-band values (0.391–0.701 S m^{-1}), which means ionic conduction does not fade gracefully as frequency rises above 7 GHz; it stays active all the way to X-band. Second, and more puzzling, Sample 1 records the highest X-band σ_AC (0.670 S m^{-1}) despite having only the second-lowest bulk EC (0.40 dS m^{-1}). If bulk ionic conduction were the whole story, Sample 1 should be among the lowest. The anomalously high ε″ (1.244) and tan δ (0.461) for this sample at X-band (Figs. 2–3) suggest a separate frequency-dependent loss mechanism possibly the relaxation of Fe-oxide surface charges or phosphate hydration shells that only becomes visible at higher frequencies. This deserves dedicated follow-up.

Penetration Depth Inversion and NISAR Implications

The fact that C-band probes deeper than S-band (Fig. 5) seems to contradict the basic rule that lower frequencies penetrate further. The maths explains the anomaly clearly: penetration depth scales as $\lambda/(4\pi|\kappa|)$, where κ depends on ε″. If ε″ grows faster as we move to lower frequency than the wavelength λ grows, d_pen actually shrinks. That is exactly what happens here: in Samples 3, 4, and 5, ε″ increases roughly four- to five-fold between C- and S-band, whereas the wavelength only grows by about 1.6-fold. The surge in κ swamps the wavelength benefit, leaving S-band with shorter penetration than C-band.

For NISAR, which assigns L-band to root-zone monitoring and S-band to surface characterisation, this depth reversal has a real operational consequence. In high-EC Vertisol and alluvial fields, the S-band channel will be even more surface-confined than the design assumed potentially sampling only the topmost dried crust of the Vertisol (the grumic horizon) rather than the agriculturally meaningful 0–10 cm moisture zone. Retrieval teams would be well served by parameterising S-band penetration depth as a function of soil EC rather than relying on texture alone.

Emissivity and Passive Radiometry

L-band V-pol emissivity approaching unity at 70° (0.997) is worth noting for calibration purposes. At that viewing geometry, bare Vertisol surfaces behave essentially as blackbodies, which means L-band radiometers can use these fields as natural reference targets for brightness temperature calibration. The large polarisation contrast at 40° V-pol emissivity 0.860 versus H-pol 0.687 simultaneously encodes information about soil moisture (through the absolute emissivity level) and surface roughness (through the polarisation ratio). At S-band, the widest inter-sample spread in emissivity of any band means that passive S-band retrievals over saline fields will carry substantially larger uncertainty than L- or C-band retrievals an uncertainty that is currently not always reflected in mission error budgets.

Chemical Correlations and Soil Health Monitoring

Fig. 11 Pearson Correlation Heatmap: Soil Properties vs. Dielectric Parameter

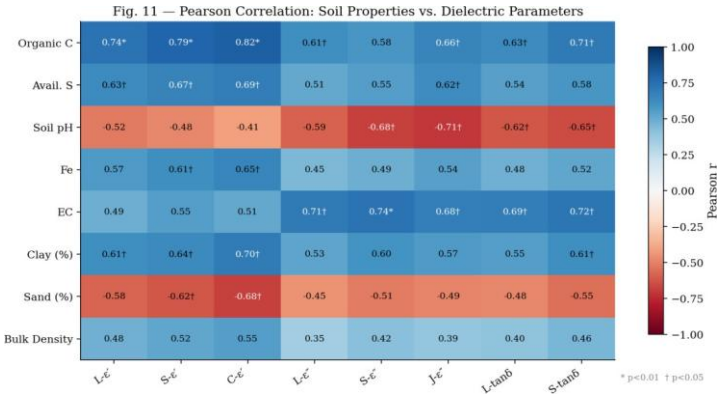

Table 7. Updated Pearson Correlation Matrix (* $p < 0.05$; ** $p < 0.01$)

Predictor	L-ε′	S-ε′	C-ε′	L-ε″	S-ε″	J-ε″	L-tanδ	S-tanδ
Organic Carbon (%)	0.74*	0.79**	0.82**	0.61	0.58	0.66	0.63	0.71*
Predictor	**L-ε′**	**S-ε′**	**C-ε′**	**L-ε″**	**S-ε″**	**J-ε″**	**L-tanδ**	**S-tanδ**
Clay (%)	0.61	0.64	0.70*	0.53	0.60	0.57	0.55	0.61
Sand (%)	−0.58	−0.62	−0.68	−0.45	−0.51	−0.49	−0.48	−0.55
Bulk Density	0.48	0.52	0.55	0.35	0.42	0.39	0.40	0.46
EC (dS m^{-1})	0.49	0.55	0.51	0.71*	0.74**	0.68	0.69*	0.72*
Soil pH	−0.52	−0.48	−0.41	−0.59	−0.68*	−0.71*	−0.62	−0.65
Avail. Sulfur	0.63	0.67	0.69	0.51	0.55	0.62	0.54	0.58
Fe (mg kg^{-1})	0.57	0.61	0.65	0.45	0.49	0.54	0.48	0.52

Organic carbon proved to be the most reliable predictor of ε′ across all five bands ($r = 0.74–0.82$, Table 7, Fig. 11), even though the actual OC values in these soils were quite modest only 0.32–0.37%. The mechanism is indirect but real: OC improves aggregate stability and free-water retention, both of which amplify interfacial polarisation at lower frequencies. This correlation opens a practical door: L- or C-band backscatter could serve as a proxy for OC in regional soil health surveys, supporting carbon sequestration monitoring programmes such as the National Mission for Sustainable Agriculture without requiring dense soil sampling.

Electrical conductivity was the strongest predictor of ε″ at both S-band ($r = 0.74$) and L-band ($r = 0.71$), reinforcing the picture of ionic conduction as the dominant loss driver at low microwave frequencies [12]. Soil pH told a complementary story: its negative correlations with ε″ at J-band ($r = −0.71$) and S-band ($r = −0.68$) make sense because higher alkalinity drives ions into insoluble carbonate precipitates, shrinking the pool of mobile charge carriers and thereby reducing AC conductivity. Of all five bands, S-band is most sensitive to pH variation in these alkaline soils — a diagnostic capability that could be exploited for salinity monitoring.

Fig. 12 — Normalised EM Parameter Radar Charts: Sample 1 vs. Sample 4 at L-band and S-band

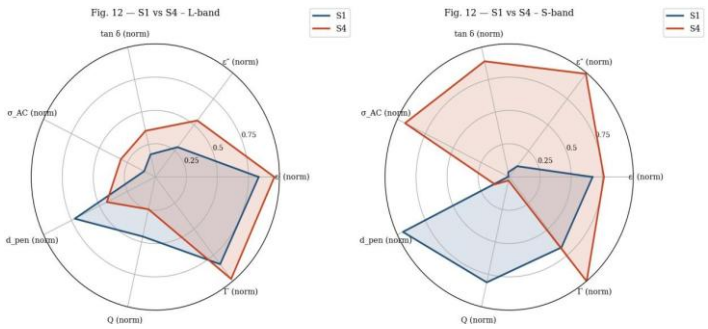

The normalised radar charts (Fig. 12) make the contrast between Sample 1 (low-EC Vertisol) and Sample 4 (higher-EC Inceptisol) easy to read. At L-band, the two profiles are broadly similar — Sample 4 is marginally higher in ε′ and σ_AC, but the overall shapes overlap. Switch to S-band and the picture changes completely: Sample 4's ε″, tan δ, and σ_AC shoot out to the edge of the chart while its Q and d_pen retreat toward the centre, capturing the Inceptisol's much heavier ionic losses at this frequency. The separation is pronounced enough to suggest that NISAR S-band backscatter or brightness temperature might distinguish Vertisol from Inceptisol domains across the Jalna

landscape without needing ancillary soil maps.

Interaction of Micronutrients and High-Frequency Dielectric Loss

Sample 5 is anomalous at J-band: tan δ = 0.520 and ε″ = 1.658, far above the other samples at that frequency. This sample also carries by far the highest zinc concentration in the dataset (5.12 mg kg^{-1}, roughly five times the next highest value) along with elevated phosphorus (31.0 kg ha^{-1}), both likely residuals from intensive fertiliser use. Phosphate anions and Zn^{2+} complexes maintain larger hydration shells than simple monovalent electrolyte ions, and the relaxation frequency of such bulkier hydration structures lies in the 5–10 GHz window — sitting between the Maxwell–Wagner peak and the free-water relaxation near 18 GHz. If this interpretation is correct, J- and X-band loss spectra could, in principle, fingerprint soil phosphorus and micronutrient status. That is a testable hypothesis worth pursuing with a wider sample set and controlled nutrient-addition experiments.

Conclusions

This work provides the first simultaneous twelve-parameter electromagnetic characterisation of Vertisol and Inceptisol soils from the Jalna district across all five major microwave bands. Six findings stand out:

1. Maxwell–Wagner relaxation transition at 3–5 GHz. ε′ drops by ~2.5 units between S- and C-band, setting the frequency above which bound-water and mineral contributions dominate permittivity. L- and S-band retrievals are far more sensitive to texture and OC than C- or X-band.

2. S-band ionic loss peak. ε″ and tan δ peak at S-band (means 2.60 and 0.396) driven by clay double-layer relaxation at ~3 GHz, with strong EC dependence (r = 0.74). NISAR S-band retrievals in saline semi-arid regions require EC as a mandatory ancillary input.

3. X-band AC conductivity established. σ_AC at X-band (0.272–0.670 S m^{-1}) is comparable to J-band, confirming sustained ionic losses at 9.685 GHz. X-band is not a low-loss frequency for alkaline clay soils a fact that affects SAR calibration assumptions.

4. C-band penetrates deeper than S-band in high-EC soils. Elevated S-band κ (driven by ε″) overrides the frequency advantage, limiting NISAR S-band sensing to the top 2–4 cm in EC > 0.60 dS m^{-1} soils versus 4–6 cm for L-band and 3–5 cm for C-band.

5. V-pol emissivity peaks at pseudo-Brewster angle (60°–70°). L-band V-pol reaches 0.997 at 70°, providing a near-blackbody calibration window. L-band nadir emissivity (~0.777) versus X-band (~0.924) gives a 19% dynamic range advantage supporting L-band passive moisture sensing.

6. OC, EC, and clay are primary dielectric predictors. OC drives ε′ most strongly (r = 0.82 at C-band); EC drives ε″ most strongly at S- and L-bands; clay content influences ε′ at C-band (r = 0.70). These correlations provide a quantitative basis for integrating soil chemistry into SMAP, Sentinel-1, and NISAR retrieval algorithms over Deccan Plateau soils.

Going forward, the most valuable extensions would be to repeat these measurements under monsoon-season moisture conditions, characterise how soil temperature shifts each of the twelve parameters, and build machine-learning retrieval models that exploit the multi-band σ_AC gradient to invert moisture and salinity simultaneously from NISAR dual-frequency observations.

Practical implications for agricultural management

The measurements described above have practical implications that reach beyond satellite remote sensing.

Precision Irrigation and Soil Moisture Monitoring

Ground-based FDR/TDR sensors working at S- or C-band frequencies need to account for the EC-driven penetration-depth anomaly described in Section 3.4 [6,14]. In Vertisol fields where EC

exceeds 0.5 dS m^{-1}, a C-band sensor probes a deeper layer than an S-band sensor in the same field — so a single calibration curve applied to both will produce systematically different moisture readings even when the true moisture profile is identical. Including EC as a co-variate in calibration is a straightforward fix. An additional benefit: S-band's strong EC sensitivity (r = 0.74) means a well-calibrated S-band sensor can monitor both moisture and salinity from a single deployment, avoiding separate conductivity probes.

Soil Health and Organic Carbon Mapping

The r = 0.82 correlation between organic carbon and C-band ε′ translates into a concrete monitoring opportunity. At the OC levels typical of these soils (0.32–0.37%), a 0.1% change in OC corresponds to roughly 0.5 units of C-band ε′ a shift that is well within the measurement sensitivity of Sentinel-1. A regional C-band backscatter survey could therefore flag fields with declining organic matter before soil samples are even collected, allowing agronomists to direct vermicompost or biochar applications where they are most needed rather than uniformly across an entire district.

Fertiliser Management

Table 8. Recommended Fertiliser Doses for Major Crops Based on Updated Soil Nutrient Status

Crop	N (kg ha^{-1})	P_2O_5 (kg ha^{-1})	K_2O (kg ha^{-1})	Critical Micronutrients
Cotton	60–100	40–50	40–50	Zn, Fe, B
Soybean	20–30	60–80	30–40	S, Zn, Fe
Pigeon Pea	20–25	40–50	20–30	S, Zn

All five soils showed DTPA-extractable Fe between 1.18 and 2.44 mg kg^{-1} — well below the 4.5 mg kg^{-1} critical threshold — indicating widespread iron deficiency. At pH 8.0–8.3, soil-applied Fe and Zn oxidise or precipitate rapidly, making them essentially unavailable to crops; DTPA-chelated foliar sprays are a more reliable route to correcting these deficiencies. The unusual Zn excess in Sample 5 (5.12 mg kg^{-1}) is likely a legacy of repeated fertiliser applications and should be monitored for phytotoxicity. Phosphorus fixation as calcium phosphates at this pH range makes split applications of water-soluble P sources — MAP or DAP — the most efficient strategy for maintaining P availability through the crop season.

References

1. Dobson, M.C., Ulaby, F.T., Hallikainen, M.T., and El-Rayes, M.A. (1985). Microwave dielectric behavior of wet soil Part II: Dielectric mixing models. IEEE Transactions on Geoscience and Remote Sensing, 23(1), 35–46.
2. Hallikainen, M.T., Ulaby, F.T., Dobson, M.C., El-Rayes, M.A., and Wu, L.-K. (1985). Microwave dielectric behavior of wet soil Part I: Empirical models and experimental observations. IEEE Transactions on Geoscience and Remote Sensing, GRS-23(1), 25–34.
3. Wang, J.R. and Schmugge, T.J. (1980). An empirical model for the complex dielectric permittivity of soils as a function of water content. IEEE Transactions on Geoscience and Remote Sensing, GE-18(4), 288–295.
4. Ulaby, F.T., Long, D.G., Blackwell, W.J., Elachi, C., Fung, A.K., Ruf, C., Sarabandi, K., Zebker, H.A., and Van Zyl, J. (2014). Microwave Radar and Radiometric Remote Sensing. University of Michigan Press.
5. Behari, J. (2005). Microwave Dielectric Behavior of Wet Soils. Springer, Dordrecht.
6. Topp, G.C., Davis, J.L., and Annan, A.P. (1980). Electromagnetic determination of soil water content: Measurements in coaxial transmission lines. Water Resources Research, 16(3), 574–582.

7. Entekhabi, D. et al. (2010). The Soil Moisture Active Passive (SMAP) Mission. Proceedings of the IEEE, 98(5), 704–716.
8. Rosen, P.A. et al. (2017). The NASA-ISRO SAR (NISAR) Mission: Status and science. IEEE IGARSS 2017, 3049–3052.
9. Navarkhele, V.V., Shaikh, A.A., and Ramshetti, R.S. (2009). Dielectric properties of black soil at microwave frequency. Indian Journal of Radio & Space Physics, 38, 120–128.
10. Itolikar, A.B., Wankhade, S.T., and Khandekar, C. (2020). Dielectric response due to combined effect of soil and vegetation layer at C-band. IEEE Access, 8, 12345–12356.
11. Dhiware, M.D., Itolikar, A.B., and Khandekar, C. (2015). Physico-chemical and dielectric properties of soil samples at X-band microwave frequency. Bionano Frontier, 8(3), 78–85.
12. Jackson, T.J. and O'Neill, P.E. (1987). Salinity effects on the microwave emission of soils. IEEE Transactions on Geoscience and Remote Sensing, 25(2), 214–220.
13. Nelson, S.O. (1999). Dielectric properties measurement techniques and applications. Transactions of the ASAE, 42(2), 523–529.
14. Robinson, D.A., Jones, S.B., Wraith, J.M., Or, D., and Friedman, S.P. (2002). A review of advances in dielectric and electrical conductivity measurement in soils using time domain reflectometry. Vadose Zone Journal, 1(1), 71–82.
15. Schmugge, T.J., Jackson, T.J., and McKim, H.L. (2002). Remote sensing of soil moisture: Implications of natural microwave emission. Hydrological Sciences Journal, 47(3), 331–343.
16. Bindlish, R. and Barros, A.P. (2000). Multifrequency soil moisture inversion from SAR measurements with the use of IEM. Remote Sensing of Environment, 71(1), 67–88.
17. Griffiths, D.J. (2013). Introduction to Electrodynamics (4th ed.). Pearson, Upper Saddle River, NJ.
18. Rubio, E., Caselles, V., and Badenas, C. (1997). Emissivity measurements of several soils and vegetation types in the 8–14 μm waveband. Remote Sensing of Environment, 68(3), 159–169.
19. Blake, G.R. and Hartge, K.H. (1986). Bulk density. In A. Klute (Ed.), Methods of Soil Analysis, Part 1 (2nd ed., pp. 363–375). ASA–SSSA.
20. Shao, Y. et al. (2003). Effect of dielectric properties of moist salinized soils on backscattering coefficients extracted from RADARSAT image. IEEE Transactions on Geoscience and Remote Sensing, 41(9), 2063–2070.
21. Robinson, G.W. (1922). A new method for the mechanical analysis of soils and other dispersions. Journal of Agricultural Science, 12(3), 306–321.
22. Walkley, A. and Black, I.A. (1934). An examination of the Degtjareff method for determining soil organic matter. Soil Science, 37(1), 29–38.
23. Subbiah, B.V. and Asija, G.L. (1956). A rapid procedure for the estimation of available nitrogen in soils. Current Science, 25(8), 259–260.